Research Article | Vol. 28, No. 14 / 6 July 2020 / Optics Express 21121
Optics EXPRESS

Combined use of TDLAS and LIBS for reconstruction of temperature and concentration fields

JUNGWUN LEE,[1,3] CHEOLWOO BONG,[1,3] JIHYUNG YOO,[2,4] AND MOON SOO BAK[1,5]

[1]School of Mechanical Engineering, Sungkyunkwan University, Suwon, 16419, South Korea
[2]Department of Automotive Engineering, Hanyang University, Seoul, 04763, South Korea
[3]Co-first authors with equal contribution
[4]jihyungyoo@hanyang.ac.kr
[5]moonsoo@skku.edu

Abstract: A new technique is developed for reconstructing the temperature and species-concentration fields by employing tunable diode laser absorption spectroscopy (TDLAS) and laser-induced breakdown spectroscopy (LIBS) on axisymmetric combustion fields. For two-line thermometry, the uncertainties in linestrengths of the absorption lines may cause systematic errors in temperature and species concentration estimations. Thus, the radial profiles of water vapor concentration are obtained first using the LIBS, assuming that the combustion is complete; then, the radial temperature profiles are estimated from the radial profiles of absorption coefficient, as reconstructed from the absorbance profiles obtained using the TDLAS. The spectral lines of water vapor at 7185.6 and 7444.36 cm^{-1} are selected as the linestrengths show monotonic decreases with the increase in temperature within the measuring temperature range. The radial profiles of temperature and water mole fraction are well-reconstructed, and the measurement error is found to be as low as 3%. The technique yielded higher temperatures compared to the thermocouple, possibly owing to the significant radiative heat loss in the thermocouple data.

1. Introduction

Temperature and species concentration are two important flow field properties for analyzing combustion phenomena. Commonly used thermometric and speciation techniques are thermocouple and gas chromatography (GC), respectively. However, these techniques require probes to protrude into the flow field and contact the sample. Consequently, the probes may often inhibit and perturb the physical and chemical processes within the flow field of interest, as well as introduce measurement errors due to the unintended conductive heat exchange via thermocouple wires or chemical reactions within the GC sampling probe. Furthermore, thermocouples are prone to significant inaccuracies at higher temperatures owing to considerable radiative heat loss to the surroundings and can therefore underpredict the temperature by a large margin. Thus, non-contact measurements of temperature and species mole fractions have been studied extensively.

Non-contact measurement methods can be classified into two types: acoustical and optical methods. Acoustical methods have been limited to thermometry [1–3] and are based on the fact that the speed of sound is a function of temperature. For implementation, a point source is used to produce acoustic waves, and the receivers detect the arrival times of the waves. As the travel time is cumulative along the propagation path, temperature fields can be obtained by reconstruction using tomography, and the measurement accuracy depends on a number of different acoustic paths [4]. Optical methods include Rayleigh scattering [5–7], Coherent anti-Stokes Raman spectroscopy (CARS) [8–10], tunable diode laser absorption spectroscopy (TDLAS) [11–16], and laser-induced breakdown spectroscopy (LIBS) [17–24], which are all based on various modes of

#396909 https://doi.org/10.1364/OE.396909
Journal © 2020 Received 14 May 2020; revised 24 Jun 2020; accepted 24 Jun 2020; published 1 Jul 2020

Optics EXPRESS

light-matter interaction, such as scattering, absorption, and emission. In combustion diagnostics, Rayleigh scattering and CARS are used to measure temperature, LIBS is used to measure local equivalence ratios, and TDLAS is used to probe both temperature and species concentration.

TDLAS measures the wavelength-dependent absorption of a laser light through a gas medium, and line-integrated absorbance is provided as the product of mole fraction of a measuring species, linestrength, pressure, and optical path length. Because the linestrength is a function of temperature and the lower energy levels affect the temperature dependence of the corresponding linestrength, a pair of absorptions lines with dissimilar lower energy levels is selected to infer temperature (so-called two-line thermometry). Here optimal absorption line selection requires lines with lower energy levels that correspond to the lower and upper bounds of the temperature range of interest, such that the absorbance ratio produces a monotonically-increasing function of temperature [12,13]. The temperature can be first determined using the absorbance ratio; then, the mole fraction is estimated for the given temperature. However, the uncertainties in spectroscopic parameters of HITRAN database [25] such as linestrength can have a profound impact on the measurement accuracy of both temperature and species concentration.

In the field of combustion, LIBS has been used to produce laser-induced plasmas in gas medium and conduct chemical elemental analysis on the emission spectra. Because of the high temperature within the plasma, all molecules dissociate into atoms, and the atoms become ionized. The emission spectrum consists of discrete lines, and a linear relation can be found between the ratios of these lines and the equivalence ratio [18–24].

In this study, we proposed a new technique that employs both TDLAS and LIBS for the reconstruction of temperature and species concentration fields. As a proof-of-concept study, the measurements were performed on combustion gases with axisymmetric fields for temperature and mole fractions. First, the radial profiles of water mole fraction were estimated from the radial equivalence ratios obtained using the LIBS, by assuming complete combustion. Then, the radial temperature profiles were estimated from the radial profiles of absorption coefficient, as reconstructed from the absorbance profiles via the inverse Abel transform. The spectral lines of water vapor at 7185.6 and 7444.36 cm^{-1} are selected for the TDLAS. Because the absorption linestrength, with a finite lower energy level, peaked then decreased with increasing temperatures, there were two different temperatures for a given linestrength. However, the linestrengths of the selected lines peaked at 500 and 900 K, and so one-to-one correspondence between the linestrength and temperature was maintained in the temperature range of interest (i.e., T > 900 K). Finally, the radial temperature profiles were derived from the two absorption line measurements, and they were then compared to those measured by the thermocouple.

2. Absorption spectroscopy

Spectral absorbance, A_ν (unitless), of the single wavelength radiation at frequency ν through an optically-thin medium with length L is described by the Beer-Lambert relation:

$$A_\nu = -\ln\left(\frac{I}{I_0}\right) = \int_0^L k_\nu(x)dx, \tag{1}$$

where I_0 and I are the incident and transmitted laser powers (W), respectively; k_ν is the spectral absorption coefficient (cm^{-1}). The spectral absorption coefficient near the absorption line is expressed as:

$$k_\nu(x) = S_{ij}(T(x))X_{abs}(x)P\phi_\nu, \tag{2}$$

where $S_{ij}(T)$ ($cm^{-2}\cdot atm^{-1}$) is the linestrength of the transition (where i and j represent the lower and upper energy levels, respectively), X_{abs} is the mole fraction of the absorbing species (unitless), P is the total pressure (atm), and ϕ_ν (cm) is the frequency-dependent line-shape

Optics EXPRESS

function normalized such that $\int_{-\infty}^{\infty} \phi_\nu d\nu = 1$. The linestrength is proportional to the density of the absorber. Assuming that the energy level populations follow the Boltzmann distribution, the temperature-dependent linestrength is expressed as:

$$S_{ij}(T) = S_{ij}(T_{ref}) \cdot \frac{Q(T_{ref})}{Q(T)} \cdot \frac{T_{ref}}{T} \cdot exp\left[-c_2 E''_{ij}\left(\frac{1}{T} - \frac{1}{T_{ref}}\right)\right] \times \left[1 - \exp\left(\frac{-c_2 \nu_{ij}}{T}\right)\right]\left[1 - \exp\left(\frac{-c_2 \nu_{ij}}{T_{ref}}\right)\right]^{-1}, \tag{3}$$

where T_{ref} is the reference temperature of 296 K; $S_{ij}(T_{ref})$ and $Q(T_{ref})$ are the linestrength and partition function, respectively, at T_{ref}; $Q(T)$ is the partition function at the temperature of interest (T); c_2 is the second radiation constant; ν_{ij} is the wavenumber of the spectral line transition in vacuum; and E" is the lower energy level.

Integrating A_ν and k_ν over the entire line shape yields expressions for the line-integrated absorbance A and absorption coefficient K, as given by:

$$A = \int_{-\infty}^{\infty} A_\nu d\nu = \int_0^L K(x)dx \tag{4}$$

and

$$K(x) = S_{ij}(T(x))X_{abs}(x)P. \tag{5}$$

In this study, the absorption lines at 7185.6 and 7444.36 cm^{-1} were employed, and their spectroscopic parameters are listed in Table 1. Each of the lines appeared as a single line, but in fact was the overlaps of three spectral lines with different lower energy levels. Figure 1 shows the sum of the linestrengths near 7185.6 and 7444.36 cm^{-1} as a function of temperature ranging from 300 to 2500 K. The linestrengths at 7185.6 and 7444.36 cm^{-1} peaked at around 500 and 900 K, respectively, then decreased with the increase of temperature. The slope of the temperature dependence was steeper for 7185.6 cm^{-1} than that of 7444.36 cm^{-1}.

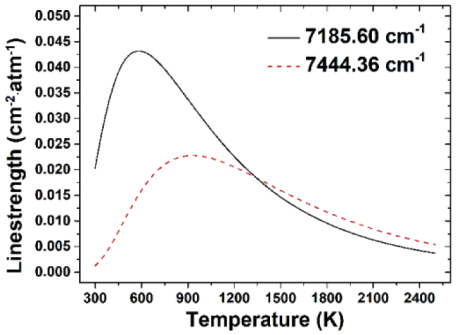

Fig. 1. Temperature dependences of linestrengths of water vapor at 7185.6 and 7444.36 cm^{-1}.

Table 1. Spectroscopic parameters of the H_2O absorption lines used in the study

Line index	Wavenumber (cm^{-1})	Linestrength at T_{ref} (cm^{-2}·atm^{-1})	Lower-state energy (cm^{-1})
1	7185.577	5.344E-05	446.51
	7185.5966	4.902E-03	1045.06
	7185.5973	1.471E-02	1045.06
2	7444.3518	5.406E-04	1774.75
	7444.3682	1.539E-04	1806.67
	7444.3706	4.620E-04	1806.67

Optics EXPRESS

3. Experimental details

Figure 2 shows the experimental setup for TDLAS and LIBS measurements on combustion fields. A flat flame burner (McKenna burner) was used to create axisymmetric temperature and species-concentration fields. The burner surface consisted of two concentric discs (made of sintered stainless steel and sintered bronze) and a 1/2-inch-diameter nozzle (inactive for this study) at the center. The outer diameters of the two discs were 60 and 70 mm, respectively. A premixed methane-air mixture was flowed through the inner disc, and the air was injected through the outer disc. In the experiments, the air flowrates through the inner and outer discs were fixed at 20 and 10 slpm, respectively, whereas the methane flowrate was varied from 1.53 to 2.12 slpm to study the different conditions of fuel-air equivalence ratio from 0.73 to 1.01.

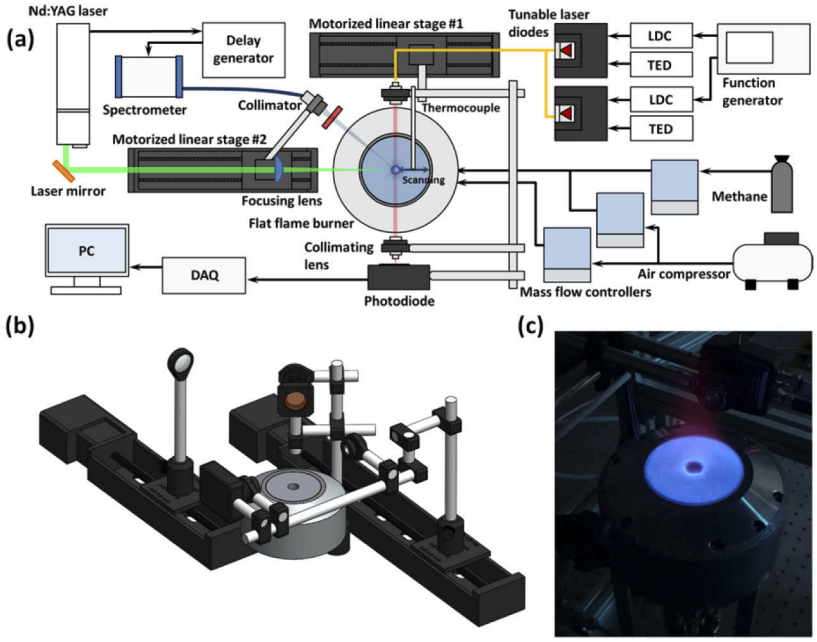

Fig. 2. (a) Schematic of TDLAS and LIBS setups on flat flame burner. (b) 3-D rendering image of the setup. (c) Photograph of the flat flame above the burner.

Two fiber-coupled tunable single-frequency lasers (EP1391-9-DM-B01-FM and EP1343-3-DM-B01-FA, Eblana Phtotonics) were employed for TDLAS. The lasers were placed on individual butterfly mounts (Thorlabs LM14S2) and their wavenumbers were tuned at a repetition rate of 10 Hz by ramp modulating the injection currents for the desired transitions near 7185.6 and 7444.36 cm^{-1}. The currents were supplied using current controllers (Thorlabs LDC201CU) connected to a function generator (GW INSTEK AFG-2225), while the temperatures were fixed using temperature controllers (Thorlabs TED200C). The laser outputs were combined using an optical coupler (Newport F-CPL-B12355-FCAPC) and were collimated using a collimator (Thorlabs TC12APC-1310). Then, the light transmitted through the gas medium was detected using a photodetector (Thorlabs PDA20CS2). During the experiments, the ramp voltages were driven below a certain threshold (i.e., there was no injection current, and the laser did not lase) and were phase-shifted by 180° to prevent the overlap of absorption signals that resulted from different lasers. The signals were recorded using an analogue input module (National Instruments NI9239) with a vertical resolution of 24-bit and a sampling rate of 50 kS/s. Radial absorbance profiles were obtained by mounting the collimator and the photodetector on a motorized linear stage (Zaber LSQ series). The total path length was measured to be 13.7 cm. For each location

Optics EXPRESS

and test conditions, absorbance data were acquired for 5 s, resulting in a total of 50 spectra for each absorption line.

The light source of LIBS was a Nd:YAG laser (Nano LG300-10, Litron Lasers) with 532-nm wavelength, 10-Hz repetition rate, 6-ns duration, and 5-mm beam diameter. The laser output was measured to be 100 mJ/pulse using a laser power meter (Thorlabs PM100USB and ES220C). The beam was focused with a plano-convex lens (Thorlabs) with a focal length of 17.5 cm to produce the laser-induced plasma. The plasma emissions were collected by a fiber-coupled collimating lens equipped with a long-pass filter with a cut-on wavelength of 570 nm (Thorlabs FGL570) to filter out the diffusive laser light scatter, and were then routed to a spectrometer (AvaSpec-ULS2048L-USB2). Similar to the TDLAS diagnostics setup, all the optics were placed on a separate motorized linear stage (Zaber LSQ series). The spectral range of the spectrometer was from 200 to 1160 nm with a resolution of 2.5 nm. Because the emission persisted for a few microseconds, a line charge-coupled device (CCD) of the spectrometer was time-synchronized to the laser using a delay generator (Quantum composer 9524). The CCD was triggered 113.55 μs before the laser firing, and the exposure time of the CCD was set to 5 ms to capture the entire plasma emission. Each LIBS measurement was obtained by averaging 100 emission spectra to enhance the signal-to-noise ratio (SNR). Lastly, the spectrometer was calibrated using a calibration light source (AvaLight-HAL-CAL-Mini).

An independent temperature measurement of the flow field was also conducted by traversing an uncoated 1-mm-diam bead-size type B thermocouple. The thermocouple was mounted on the same linear stage used for the TDLAS measurements.

4. Results and discussion

The radial temperature profiles were obtained using the type B thermocouple (as references) for equivalence ratios from 0.73 to 1.01, as shown in Fig. 3. For all equivalence ratios, the temperatures were nearly constant when the radius (r) was less than 20 mm but decreased rapidly for $20 < r < 36$ mm, as the combustion gas mixes with the surrounding air co-flow. As the equivalence ratio increased, the average temperature increased from 1476 to 1585 K for $0 < r < 20$ mm. The temperatures were slightly lower at the center because no gas was injected through the nozzle. The combustion gases will be stagnated in the region while losing heat to the burner surface. It is noteworthy that the obtained temperatures are not radiation-corrected and turned out to be significantly lower than those from the optical measurements.

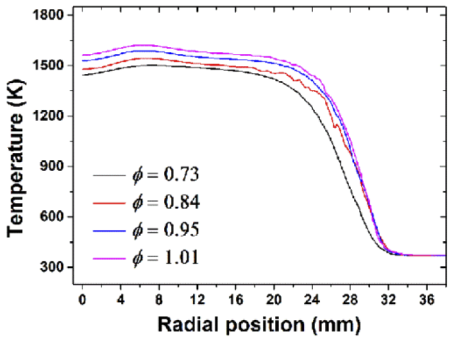

Fig. 3. Radial temperature profiles measured by type B thermocouple for equivalence ratios from 0.73 to 1.01.

The TDLAS measurements were then conducted 7 mm above the burner surface. Figure 4(a) and (b) show the transmitted laser intensities scanned for wavenumbers near 7185.6 and 7444.36 cm^{-1}, respectively. The absorbances were calculated using Eq. (1) while the incident laser

Optics EXPRESS

intensities are represented by the red lines in Figs. 4(a) and 4(b) (i.e., baselines) assuming that the laser intensity changes linearly with the wavenumber. The absolute wavenumbers were calibrated by matching the absorbance profiles to the corresponding theoretical spectra synthesized using HITRAN 2016 database, as shown in Figs. 4(c) and 4(d). The conditions for the measured spectra are r = 0 mm and $\phi = 0.73$, and those for the theoretical spectra near 7185.6 and 7444.36 cm^{-1} are $T = 1735$ and 1885 K, respectively, at $X_{H2O} = 0.139$, $L = 5.6$ cm, and $P = 1$ atm. The measured spectra were found to agree well with the theoretical results, but the line shape of 7444.36 cm^{-1} seemed slightly broader. This was attributed to either uncertainties in broadening coefficients of the lines, or the fact that the laser absorption was a line-of-sight measurement and so the non-uniform radial distributions of temperature and water mole fraction may deviate the line shapes from those of a set of single T, X_{H2O}, L, and P. Thus, in this study, we integrated the spectral lines at 7185.6 and 7444.36 cm^{-1} to avoid the effect of line shape on the estimation of temperature and water mole fraction. The spectral lines were first fitted with the Voigt function of a single transition, although each line was in fact a result of the overlap of three spectral lines with different lower energy levels. The areas of the fitted lines were then calculated for integrated absorbance (see Eq. (4)).

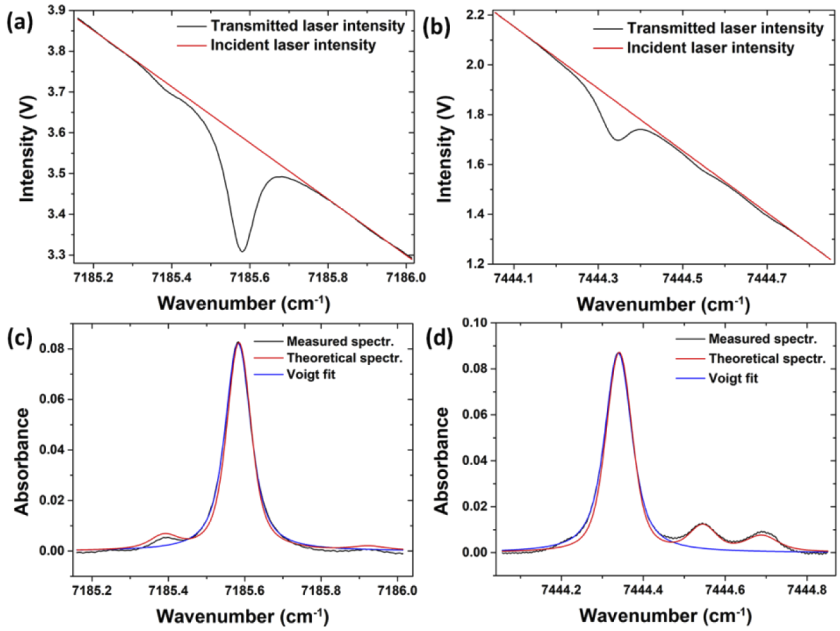

Fig. 4. Incident and transmitted laser intensities near (a) 7185.6 cm^{-1} and (b) 7444.36 cm^{-1}; spectral absorbances near (c) 7185.6 cm^{-1} and (d) 7444.36 cm^{-1} with their theoretical spectra and Voigt fits.

Figures 5(a) and 5(b) show the line-integrated absorbances at 7185.6 and 7444.36 cm^{-1}, respectively, as functions of the closest distance from the laser beam to the burner axis for equivalence ratios from 0.73 to 1.01. Because, in general, the water vapor concentration is higher in high-temperature region, the absorbances increases as the laser path covered the combustion region more. It seemed that the absorbances increased slightly with the equivalence ratio, but this may not necessarily be the case since the linestrengths decrease with the temperature in the measuring range whereas the absorption coefficients increase proportionally with the water mole fraction. Interestingly, the absorbances at 7444.36 cm^{-1} decayed to zero for r > 32 mm whereas those at 7185.6 cm^{-1} remained finite (i.e., approximately 1.5×10^{-3}). This was because of the

Optics EXPRESS

humidity of the room air and the fact that the linestrength at 7185.6 cm^{-1} and 300 K was still half of its peak value whereas the linestrength at 7444.36 cm^{-1} and 300 K was nearly zero.

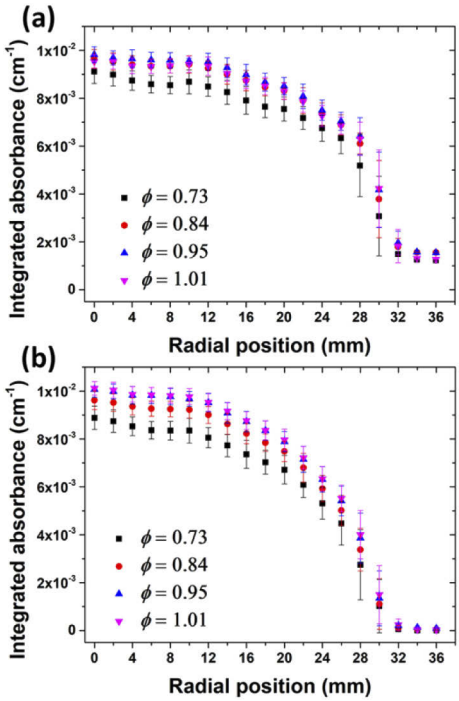

Fig. 5. Integrated absorbances at (a) 7185.6 cm^{-1} and (b) 7444.36 cm^{-1}, as a function of the closest distance between the laser beam and burner axis for equivalence ratios from 0.73 to 1.01.

The error bars in Fig. 5 were quite large. As the measurements were repeated at 10 Hz for 5 s, the integrated absorbances of each wavenumber are plotted in Figs. 6(a), 6(b), 6(c), and 6(d) as a function of time. The conditions for the curves were $\phi = 0.73$, 0.84, 0.95, and 1.01, respectively, at r = 0 mm. The absorbances oscillated sinusoidally for all measurement positions and equivalence ratios, and the oscillations at the two wavenumbers were 180° out of phase for each condition (i.e., the absorbance showed peaks for 7185.6 cm^{-1} and troughs for 7444.36 cm^{-1}). Their fitted sinusoidal curves are also shown in Fig. 6. For the same equivalence ratio, the frequencies of the oscillations were all the same but the amplitudes were larger in the region where the combustion gas mixes with the air co-flow (data not shown). Recalling that the linestrength at 7185.6 cm^{-1} decreased while that at 7444.36 cm^{-1} increased for temperatures from 500 to 900 K, we expected that these oscillations were caused by the periodic formation of toroidal vortices under the shear between the combustion gas and surrounding air streams, resulting in the periodic mixing and cooling of the region. Notably, the frequency of the oscillation decreased with the equivalence ratio (i.e., with the increase of the temperature and flow speed of the combustion gas).

The three-point Abel inversion [26] was performed on integrated absorbances for each wavenumber after phase-synchronizing the oscillations at all positions for the given equivalence ratios and removing the effect of room air humidity on the absorbances, particularly at 7185.6 cm^{-1}. Figures 7(a) and 7(b) show the line-integrated radial absorption coefficients at 7185.6 and 7444.36 cm^{-1}, respectively, for equivalence ratios from 0.73 to 1.01. For all equivalence ratios, large error bars appear only in the region with $28 < r < 32$ mm. Recalling that the absorbance showed peaks at 7185.6 cm^{-1} and troughs at 7444.36 cm^{-1}, the shape of the profile of absorption

Optics EXPRESS

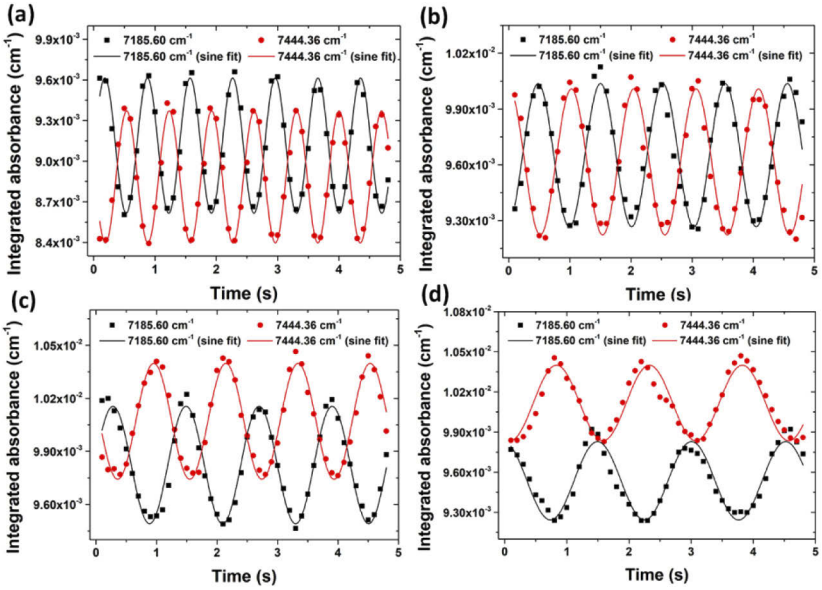

Fig. 6. Time-varying integrated absorbances at 7185.6 and 7444.36 cm^{-1} measured at the burner center for different equivalence ratios of (a) 0.73, (b) 0.84, (c) 0.95, and (d) 1.01.

coefficient for 7185.6 cm^{-1} expands (or shrinks) radially, while it shrinks (or expands) for 7444.36 cm^{-1}. Thus, the large error bars at all distances in Fig. 5 were because of the inclusion of this circumferential oscillation as the absorbance is the integral of the absorption coefficient along the path, and the size of the error bars (i.e., oscillatory amplitude) increased with the distance (d) from the burner axis until $d < 32$ mm as the laser beam traversed the region with a longer distance. For all shapes, the absorption coefficient increased for $r < 28$ mm, then decreased rapidly to zero until $r < 36$ mm. At the center (i.e., $r < 6$ mm), they were slightly higher than the values at $r \sim 6$ mm. The absorption coefficients varied relative to their averages more significantly for 7185.6 cm^{-1} than for 7444.36 cm^{-1}, and this was owing to the fact that the linestrength at 7185.6 cm^{-1} decays more rapidly with the temperature than that at 7444.36 cm^{-1} (see Fig. 1). Meanwhile, as the equivalence ratio increases, the absorption coefficients also increased although the increments were less than those in water mole fractions. This indicates that the linestrengths needed to be smaller and the temperatures needed to be higher for the increased equivalence ratio, which was consistent with the results from the thermocouple. The absorption coefficient is the product of the water mole fraction and temperature, and the radial profile of either the water mole fraction or temperature should be provided to determine the other unknown radial profile.

In this study, the laser-induced breakdown spectroscopy was conducted at the same downstream location (7 mm from the burner surface) for varying the radial distance from the burner center and equivalence ratio. Figure 8(a) shows the emission spectra of the laser-induced plasmas at equivalence ratios from 0.73 to 1.01. Because the spectra may vary with different optical setups, they were first measured for combusted gas streams of known equivalence ratios. In Fig. 8(a), the spectra are all normalized to the atomic oxygen line at 777 nm. The atomic hydrogen line at 656 nm increased with the equivalence ratio. The ratio of H line-intensity at 656 nm to O line-intensity at 777 nm is plotted as a function of equivalence ratio in Fig. 8(b). There was a strong linear propensity between the H/O line-intensity ratio and the equivalence ratio, although the gas temperature increased with the equivalence ratio. The diagnostic technique was solely to measure the local equivalence ratio rather than a mole fraction of a specific gas, temperature, or

Optics EXPRESS

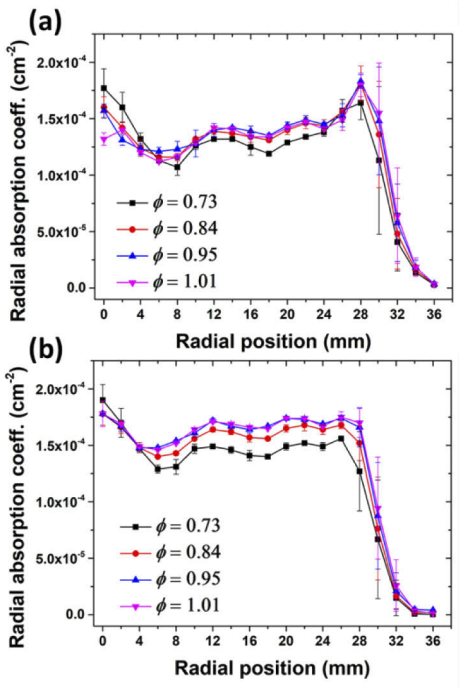

Fig. 7. Radial profiles of absorption coefficient reconstructed using three-point Abel inversion at (a) 7185.6 cm^{-1} and (b) 7444.36 cm^{-1}.

density. This was shown in detail in the previous studies [18], in which the breakdown emission spectra were recorded with an exposure time less than 2 ns while changing the time delays with reference to the laser trigger. When the combustion occurred at 1 atm, the density became sufficiently low such that the broadband emission by the inverse Bremsstrahlung process was weak and the emission was composed mainly of discrete atomic lines. In addition, the H/O line-intensity ratio was also reported as it has less sensitivity to parameters such as density, compared to other atomic intensity ratios [20], presumably because of their similar upper energy levels.

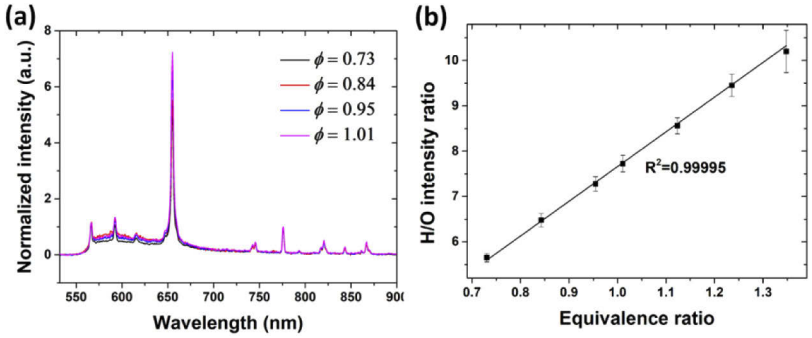

Fig. 8. (a) Emission spectra of laser-induced plasmas for equivalence ratios from 0.73 to 1.01. The spectra are normalized by the intensity of O (at 777 nm). (b) Ratio of H and O line-intensities within the spectra, as a function of the equivalence ratio.

Optics EXPRESS

When the combustion takes place, the fuel is almost completely burnt and converted into water and carbon dioxide. Although minor species such as hydrogen, carbon monoxide, and nitrogen oxides are of interest during combustion, their concentrations are typically less than 1%. Thus, by assuming that combustion was complete, we estimated the local water mole fraction from the local equivalence ratio. Figure 9 shows the radial profiles of water mole fractions for equivalence ratios from 0.73 and 1.01. For all equivalence ratios, the water mole fraction was nearly constant for r < 24 mm, including the center nozzle region, but decreased rapidly. As the equivalence ratio increases to unity, the average level of water mole fraction also increased accordingly.

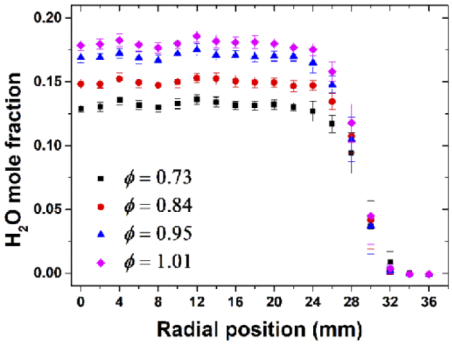

Fig. 9. Radial profiles of H_2O mole fraction obtained using LIBS for different equivalence ratios.

Finally, for the given radial profiles of the water mole fraction, the radial temperature profiles were derived from the radial absorption coefficients of each wavenumber. The radial absorption coefficients (in Fig. 7) were first divided by the water mole fractions at the same radial positions. Because the water mole fraction approached zero for r > 30 mm, the line strengths were obtained for r < 30 mm. The resulting radial linestrengths were then converted into temperatures based on the curves in Fig. 1. We note that there could be two temperature values for each linestrength, as the linestrengths at 7185.6 and 7444.36 cm^{-1} peaked at 500 and 900 K, respectively. One is higher than 500 or 900 K and the other is lower. However, the temperature range of interest was above 900 K so that the temperatures were determined for higher values. Figures 10(a) and 10(b) show the radial temperature profiles using two different data pairs: (LIBS data, TDLAS data on the spectral line at 7185.6 cm^{-1}) and (LIBS data, TDLAS data on the spectral line at 7444.36 cm^{-1}), for equivalence ratios from 0.73 to 1.01. For all equivalence ratios, the temperatures were nearly constant (i.e., varied less than 200 K) for 6 < r < 24 mm but decreased rapidly when r > 24 mm. For r < 6 mm, the temperatures were slightly lower than those for 6 < r < 24 because no gas was injected through the nozzle. As the equivalence ratio increases to unity, the average temperatures at 6 < r < 24 mm were measured to increase from 1838 to 2019 K and from 1908 to 2067 K with the spectral lines at 7185.6 and 7444.36 cm^{-1}, respectively. The temperatures for the 7444.36 cm^{-1} line were higher than those for the 7185.6 cm^{-1} line by approximately 60 K. These temperatures were quite close to the adiabatic flame temperatures for the given equivalence ratios (i.e., 1888, 2055, 2189, and 2230 K) calculated using Cantera [27] and GRI-Mech 3.0 [28], but the difference between them became larger with the increase in the equivalence. All the trends were consistent with those obtained from the thermocouple, but the absolute temperature values were significantly higher by approximately 425 K. These can be attributed to the fact that the thermocouple considerably underestimates the high temperatures as a result of radiative heat loss, and the conductive heat exchange through the wires can cause further errors [29,30]. The measurement error was found to be as low as 3%.

Optics EXPRESS

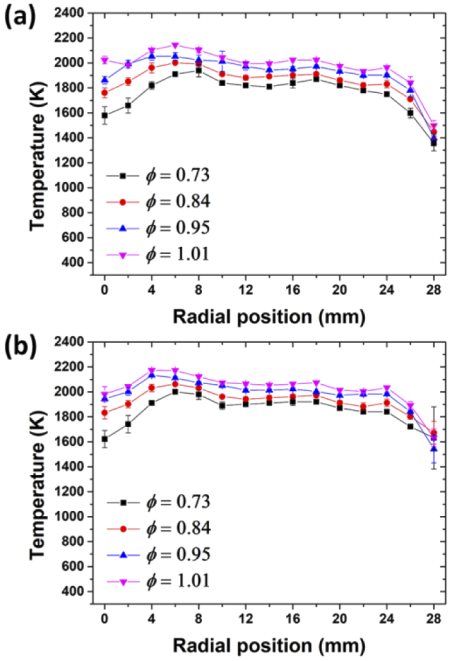

Fig. 10. Radial temperature profiles obtained using two different data pairs: (a) (LIBS data, TDLAS data on the spectral line at 7185.6 cm^{-1}) and (b) (LIBS data, TDLAS data on the spectral line at 7444.36 cm^{-1}).

Although the technique has only been applied to a steady state, axisymmetric combustion field in this study, it can be also applied to turbulent combustion fields, in which the temperature and concentration fields are 3-dimensional. This can be achieved by simultaneously conducting the TDLAS measurements for laser paths from different projection angles and the LIBS measurements at locations distributed over the measuring area.

5. Conclusions

A new technique was developed for the reconstruction of temperature and species-concentration fields by employing TDLAS and LIBS. In two-line thermometry, the uncertainties in linestrengths might lead to underestimation or overestimation of the temperature and water mole fraction. To overcome this issue, LIBS, which is a point measurement, was performed on the axisymmetric combustion fields to measure the radial profiles of the water mole fraction by assuming that the combustion was complete. Then, TDLAS, which is a line-of-sight measurement, was conducted with the same fields to estimate the radial temperature profiles. The absorption lines of water vapor at 7185.6 and 7444.36 cm^{-1} were deliberately selected as the linestrengths showed monotonic decreases with the temperature within the measuring range (i.e., $T > 900$ K). The radial profiles of the absorption coefficient were reconstructed using the Abel inversion from the path-integrated absorbances obtained by changing the distance to the burner center. The temperatures were estimated from the temperature-dependent linestrengths obtained by dividing the radial absorption coefficient by the radial water mole fraction, and the temperatures were determined to be higher than 900 K for a given linestrength. The shapes of the temperature profiles were close to those obtained from the thermocouple; however, the values were higher as the thermocouple underestimated the temperatures due to radiative heat loss. In general, the measurement errors were as small as 3%.

Optics EXPRESS

Funding

National Research Foundation of Korea (NRF-2018R1C1B6005217).

Disclosures

The authors declare no conflicts of interest.

References

1. M. Bramanti, E. A. Salerno, A. Tonazzini, S. Pasini, and A. Gray, "An acoustic pyrometer system for tomographic thermal imaging in power plant boilers," IEEE Trans. Instrum. Meas. **45**(1), 159–167 (1996).
2. Ł. Śladewski, K. Wojdan, K. Świrski, T. Janda, D. Nabagło, and J. Chachuła, "Optimization of combustion process in coal-fired power plant with utilization of acoustic system for in-furnace temperature measurement," Appl. Therm. Eng. **123**, 711–720 (2017).
3. J. Lee, C. Bong, H. Sun, J. Jeong, and M. S. Bak, "Thermometry of combustion gases using light emission and acoustic wave from laser-induced sparks," J. Phys. D: Appl. Phys. **52**(31), 315201 (2019).
4. L. Xiang, S. Tang, M. Ahmad, and L. Xing, "High Resolution X-ray-Induced Acoustic Tomography," Sci. Rep. **6**(1), 2–7 (2016).
5. F. Q. Zhao and H. Hiroyasu, "The applications of laser Rayleigh scattering to combustion diagnostics," Prog. Energy Combust. Sci. **19**(6), 447–485 (1993).
6. N. Jiang, P. S. Hsu, S. W. Grib, and S. Roy, "Simultaneous high-speed imaging of temperature, heat-release rate, and multi-species concentrations in turbulent jet flames," Opt. Express **27**(12), 17017 (2019).
7. S. W. Grib, N. Jiang, P. S. Hsu, P. M. Danehy, and S. Roy, "Rayleigh-scattering-based two-dimensional temperature measurement at 100-kHz frequency in a reacting flow," Opt. Express **27**(20), 27902 (2019).
8. S. Roy, J. R. Gord, and A. K. Patnaik, "Recent advances in coherent anti-Stokes Raman scattering spectroscopy: Fundamental developments and applications in reacting flows," Prog. Energy Combust. Sci. **36**(2), 280–306 (2010).
9. R. J. Hall, "CARS spectra of combustion gases," Combust. Flame **35**(C), 47–60 (1979).
10. R. Santagata, M. Scherman, M. Toubeix, M. Nafa, B. Tretout, and A. Bresson, "Ultrafast background-free ro-vibrational fs/ps-CARS thermometry using an Yb:YAG crystal-fiber amplified probe," Opt. Express **27**(23), 32924 (2019).
11. C. S. Goldenstein, R. M. Spearrin, J. B. Jeffries, and R. K. Hanson, "Infrared laser-absorption sensing for combustion gases," Prog. Energy Combust. Sci. **60**, 132–176 (2017).
12. D. S. Baer, E. R. Furlong, R. K. Hanson, V. Nagali, and M. E. Newfield, "Scanned- and fixed-wavelength absorption diagnostics for combustion measurements using multiplexed diode lasers," AIAA J. **34**(3), 489–493 (1996).
13. Y. Zhou, G. C. Mathews, and C. S. Goldenstein, "Compact, fiber-coupled, single-ended laser-absorption-spectroscopy sensors for high-temperature environments," Appl. Opt. **57**(25), 7117–7126 (2018).
14. L. H. Ma, L. Y. Lau, and W. Ren, "Non-uniform temperature and species concentration measurements in a laminar flame using multi-band infrared absorption spectroscopy," Appl. Phys. B: Lasers Opt. **123**(3), 83 (2017).
15. F. Wang, Q. Wu, Q. Huang, H. Zhang, J. Yan, and K. Cen, "Simultaneous measurement of 2-dimensional H_2O concentration and temperature distribution in premixed methane/air flame using TDLAS-based tomography technology," Opt. Commun. **346**, 53–63 (2015).
16. G. Gao, T. Zhang, G. Zhang, X. Liu, and T. Cai, "Simultaneous and interference-free measurements of temperature and C_2H_4 concentration using a single tunable diode laser at 1.62 μm," Opt. Express **27**(13), 17887 (2019).
17. R. Gaudiuso, M. Dell'Aglio, O. de Pascale, G. S. Senesi, and A. de Giacomo, "Laser induced breakdown spectroscopy for elemental analysis in environmental, cultural heritage and space applications: A review of methods and results," Sensors **10**(8), 7434–7468 (2010).
18. K. Kobayashi, M. S. Bak, H. Tanaka, C. Carter, and H. Do, "Laser-induced breakdown emission in hydrocarbon fuel mixtures," J. Phys. D: Appl. Phys. **49**(15), 155201 (2016).
19. S. Oh, C. D. Carter, Y. Park, S. Bae, and H. Do, "Non-intrusive laser-induced breakdown spectroscopy in flammable mixtures via limiting inverse-bremsstrahlung photon absorption," Combust. Flame **215**, 259–268 (2020).
20. J. Kiefer, J. W. Tröger, Z. Li, T. Seeger, M. Alden, and A. Leipertz, "Laser-induced breakdown flame thermometry," Combust. Flame **159**(12), 3576–3582 (2012).
21. M. Gragston, P. Hsu, A. Patnaik, Z. Zhang, and S. Roy, "Time-Gated Single-Shot Picosecond Laser-Induced Breakdown Spectroscopy (ps-LIBS) for Equivalence-Ratio Measurements," Appl. Spectrosc. **74**(3), 340–346 (2020).
22. P. S. Hsu, M. Gragston, Y. Wu, Z. Zhang, A. K. Patnaik, J. Kiefer, S. Roy, and J. R. Gord, "Sensitivity, stability, and precision of quantitative Ns-LIBS-based fuel-air-ratio measurements for methane-air flames at 1–11 bar," Appl. Opt. **55**(28), 8042 (2016).
23. A. K. Patnaik, P. S. Hsu, Y. Wu, M. Gragston, Z. Zhang, J. R. Gold, and S. Roy, "Ultrafast laser-induced-breakdown spectroscopy (LIBS) for F/A-ratio measurement of hydrocarbon flames," in *AIAA SciTech* (Kissimmee, FL, 2018).
24. Y. Wu, M. Gragston, Z. Zhang, P. S. Hsu, N. Jiang, A. K. Patnaik, S. Roy, and J. R. Gord, "High-pressure 1D fuel/air-ratio measurements with LIBS," Combust. Flame **198**, 120–129 (2018).
25. I. E. Gordon, L. S. Rothman, C. Hill, R. V. Kochanov, Y. Tan, P. F. Bernath, M. Birk, V. Boudon, A. Campargue, K. V. Chance, B. J. Drouin, J. M. Flaud, R. R. Gamache, J. T. Hodges, D. Jacquemart, V. I. Perevalov, A. Perrin, K. P.

Optics EXPRESS

Shine, M. A. H. Smith, J. Tennyson, G. C. Toon, H. Tran, V. G. Tyuterev, A. Barbe, A. G. Császár, V. M. Devi, T. Furtenbacher, J. J. Harrison, J. M. Hartmann, A. Jolly, T. J. Johnson, T. Karman, I. Kleiner, A. A. Kyuberis, J. Loos, O. M. Lyulin, S. T. Massie, S. N. Mikhailenko, N. Moazzen-Ahmadi, H. S. P. Müller, O. V. Naumenko, A. V. Nikitin, O. L. Polyansky, M. Rey, M. Rotger, S. W. Sharpe, K. Sung, E. Starikova, S. A. Tashkun, J. V. Auwera, G. Wagner, J. Wilzewski, P. Wcisło, S. Yu, and E. J. Zak, "The hitran 2016 molecular spectroscopic database," J. Quant. Spectrosc. Radiat. Transfer **203**, 3–69 (2017).

26. C. J. Dasch, "One-dimensional tomography: a comparison of Abel, onion-peeling, and filtered backprojection methods," Appl. Opt. **31**(8), 1146 (1992).
27. D. G. Goodwin, H. K. Moffat, and R. L. C. Speth, "Cantera: An object-oriented software toolkit for chemical kinetics, thermodynamics, and transport processes, version 2.4.0," Caltech: Pasadena, CA (2018).
28. G. P. Smith, D. M. G. M. Frenklach, N. W. Moriarty, B. Eiteneer, M. Goldenberg, C. T. Bowman, R. K. Hanson, S. Song, W. C. Gardiner, V. V. Lissianski, and Z. Qin, "GRI-MECH 3.0" http://combustion.berkeley.edu/gri-mech/.
29. C. Shaddix, "Correcting thermocouple measurements for radiation loss: a critical review," in *Proceedings of the 33rd National Heat Transfer Conference*, M. K. Jensen and M. di Marzo, eds. (1999).
30. V. Hindasageri, R. P. Vedula, and S. V. Prabhu, "Thermocouple error correction for measuring the flame temperature with determination of emissivity and heat transfer coefficient," Rev. Sci. Instrum. **84**(2), 024902 (2013).